Eur. Phys. J. A **21**, 155–159 (2004)
DOI 10.1140/epja/i2003-10177-0

THE EUROPEAN PHYSICAL JOURNAL A

Pion radii in the nonlocal chiral quark model

A.E. Dorokhov[a], A.E. Radzhabov[b], and M.K. Volkov[c]

Bogoliubov Laboratory of Theoretical Physics, Joint Institute for Nuclear Research, 141980 Dubna, Russia

Received: 28 November 2003 /
Published online: 13 July 2004 –
Communicated by V.V. Anisovich

Abstract. The electromagnetic radius of a charged pion and the transition radius of a neutral pion are calculated in the framework of the nonlocal chiral quark model. It is shown in this model that the vector meson contributions to the pion radii are noticeably suppressed in comparison with a similar contribution in the local Nambu–Jona-Lasinio model. The form factor for the process $\gamma^*\pi^+\pi^-$ is calculated for -1 GeV$^2<$ $q^2 < 1.6$ GeV^2. Our results are in satisfactory agreement with experimental data.

PACS. 14.40.-n Mesons – 11.10.Lm Nonlinear or nonlocal theories and models – 12.39.Ki Relativistic quark model

1 Introduction

In our works [1,2] the nonlocal chiral quark model with quark form factors of the Gaussian type was proposed. This approach is the development of the nonlocal quark models considered in [3–5]. These models are nonlocal extensions of the well-known Nambu–Jona-Lasinio (NJL) model with local quark interaction [6,7]. However, with nonlocal form factors, quark loops are free of ultraviolet (UV) divergences and it is possible to implement the quark confinement. Moreover, the nonlocal structure may be motivated [4] by fundamental QCD interactions induced by the instanton and gluon exchanges [8–10], which leads to spontaneous breaking of the chiral symmetry, solves the $U_A(1)$ problem and dynamically generates a momentum-dependent quark mass. The use of a covariant nonlocal low-energy quark model based on a self-consistent approach to the dynamics of quarks has many attractive features: it preserves gauge invariance, it is consistent with the low-energy theorems as well as takes into account the large-distance dynamics controlled by bound states [3,4, 11,12]. Masses and strong decays of the scalar, vector and axial-vector mesons were considered earlier in [1–3].

Nonlocal models, in contrast with the local NJL model, can be successfully used for the description of not only the constant part of amplitudes of meson interactions but also of the momentum expansion of amplitudes at small energies. With the help of these expansions it is possible to describe a set of important meson properties: electromagnetic radii, electric and magnetic polarizabilities, meson-meson scattering lengths, slope parameters and so on.

In the standard local NJL models [6,7] such expansions are not valid and can lead to incorrect results. In order to demonstrate this, let us consider the calculation of the pion radius. The expansion of the triangle quark diagram (fig. 3a below) with two pions and one photon connected locally to quark lines[1] leads to a satisfactory agreement with experimental data [13–15]. However, in addition, it is necessary to take into account the contribution of the diagram with the intermediate ρ-meson, fig. 3e. In the framework of the local NJL model this contribution is comparable with that of the contact diagram. As a result, we obtain a too large value for the pion radius which is in disagreement with experimental data [15]. Some authors attempted to solve this problem, using different approaches. Some of them ignored this contribution [14,16] while the others used special methods beyond the standard local NJL model [15,17,18].

In this work, we demonstrate that this problem can be solved in the framework of the nonlocal models without any additional assumption. In these models, the contribution of the diagrams with intermediate vector mesons is shown to be suppressed. It is essentially smaller than the contribution of the contact diagram. However, without ρ-meson diagrams it is impossible to describe the form factor of the process $\gamma^*\pi^+\pi^-$ in the time-like region. Our results are in satisfactory agreement with experimental data.

[a] e-mail: dorokhov@thsun1.jinr.ru
[b] e-mail: aradzh@thsun1.jinr.ru
[c] e-mail: volkov@thsun1.jinr.ru

[1] In the following this kind of diagrams will be called contact diagrams.

Notice, that similar calculations in the framework of nonlocal models of different kind were also performed in other works (see, *e.g.*, [3,11,19–21]).

2 Nonlocal quark-meson Lagrangian and model parameters

The calculations are carried out in the effective chiral model with nonlocal quark-quark interaction, which is made covariant by the inclusion of the P-exponents in the nonlocal-interaction vertex[2]. A specific prescription for the Wilson lines and their differentiation follows exactly refs. [5,11]. The nonlocal $SU(2) \times SU(2)$ symmetric quark-meson Lagrangian is given by

$$\mathcal{L}(q,\bar{q},\sigma,\pi,\rho,\omega,A) = -\frac{\pi^a(x)^2+\tilde{\sigma}(x)^2}{2G_1} \tag{1}$$
$$+\frac{(\rho^{\mu\,a}(x))^2+(\omega^\mu(x))^2}{2G_2}+\bar{q}(x)(i\hat{\partial}_x - eQ\hat{A}(x))q(x)$$
$$+\int \mathrm{d}^4x_1\mathrm{d}^4x_2\, f(x-x_1)f(x_2-x)\bar{q}(x_1)E(x_1,x)\,(\tilde{\sigma}(x)$$
$$+\pi^a(x)i\gamma^5\tau^a+\rho^{\mu\,a}(x)\gamma^\mu\tau^a+\omega^\mu(x)\gamma^\mu)\,E(x,x_2)q(x_2),$$
$$E(x,y) = \mathrm{Pexp}\left(-ieQ\int\limits_x^y A^\mu(z)\mathrm{d}z_\mu\right),$$

where τ^a are the Pauli matrices and γ^μ, γ^5 are the Dirac matrices; $\bar{q}(x) = (\bar{u}(x), \bar{d}(x))$ are the u- and d-quark fields; $\tilde{\sigma}(x)$, $\pi(x)$, $\rho(x)$, $\omega(x)$ are the σ-, π-, ρ-, ω-meson fields, respectively; $A^\mu(x)$ is the photon field; $Q = 1/2(\tau^3 + 1/3)$ is the electric charge operator, G_1, G_2 are the dimensional constants of the four-quark interaction, and $E(x,y)$ is the Schwinger phase factor.

The field $\tilde{\sigma}(x)$ has a nonzero vacuum expectation value $\langle\tilde{\sigma}\rangle_0 = \sigma_0 \neq 0$. In order to obtain a physical scalar field with zero vacuum expectation value, it is necessary to shift the scalar field as $\tilde{\sigma}(x) = \sigma(x) + \sigma_0$. In the momentum representation this leads to the appearance of the dynamical quark mass function $m(p) = -\sigma_0 f^2(p)$. From the condition of absence of the linear σ term in the Lagrangian (1) one obtains the gap equation for the dynamical quark mass

$$m(p) = f^2(p)G_1\frac{8N_c}{(2\pi)^4}\int \mathrm{d}^4_E k f^2(k)\frac{m(k)}{k^2+m^2(k)}, \tag{2}$$

where N_c is the number of colors. This and further equations are given in the Euclidean space. For numeric estimates of the nonlocal effects we shall use the momentum-dependent dynamical mass defined by condition [2]

$$\frac{m^2(p)}{m^2(p)+p^2} = \exp\left(-p^2/\Lambda^2\right). \tag{3}$$

This choice, following similar considerations given in [3,5,20], provides quark confinement. Indeed, the expression for $m(p)$ is found to be

$$m(p) = \left(\frac{p^2}{\exp\left(p^2/\Lambda^2\right)-1}\right)^{1/2}; \tag{4}$$

it depends only on one free parameter Λ, has no any singularities in the whole real axis and exponentially drops as $p^2 \to \infty$ in the Euclidean domain. From eq. (2) it follows that nonlocal form factors have similar behavior providing the absence of UV divergences in the model. At $p^2 = 0$ the mass function is equal to the cut-off parameter Λ, $m(0) = \Lambda$, which is a specific feature of the model [2]. From the gap equation we find the relation between four-quark coupling, G_1, and the nonlocality parameter, Λ ,

$$G_1 = \frac{2\pi^2}{N_c}\frac{1}{\Lambda^2}. \tag{5}$$

The expressions for meson renormalization functions are found from the consideration of meson polarization operators. For the following calculations we need only the values of these functions at $p^2 = 0$ where they take the form

$$g_\pi^{-2}(0) = \frac{N_c}{4\pi^2}\left(\frac{3}{8}+\frac{\zeta(3)}{2}\right), \qquad g_\pi(0) \approx 3.7, \tag{6}$$

$$g_\rho^2(0) = \frac{M_\rho^2}{G_2^{-1}+\Pi_\rho^T(0)}, \qquad g_\rho(0) = g_\omega(0), \tag{7}$$

where ζ is the Riemann zeta-function, $\Pi_\rho^T(p)$ is the transversal part of the ρ-meson polarization operator. In the chiral limit one has two arbitrary parameters Λ, G_2. We fix their values with help of the weak pion decay constant $f_\pi = 93$ MeV, and ρ-meson mass $M_\rho = 770$ MeV. By using the Goldberger-Treiman relation $g_\pi(0) = m(0)/f_\pi$ one finds $\Lambda = m(0) = 340$ MeV. The constant G_2 is found as $G_2^{-1} = -\Pi_\rho^T(M_\rho)$. Fitting this value to the ρ-meson mass we obtain $G_2 = 6.5$ GeV^{-2} that corresponds to the coupling $g_\rho^2(0) \approx M_\rho^2 G_2 \approx 4$.

Apart from the usual local quark-photon vertex in the Lagrangian (1) there appear quark-photon and quark-photon-meson nonlocal vertices generated by Pexp (see fig. 1). The details of calculation of these vertices can be found in [3,4,11,19]. The explicit form of the vertices appearing in the diagrams describing photon–vector-meson transitions (see fig. 2) is given in appendix A.

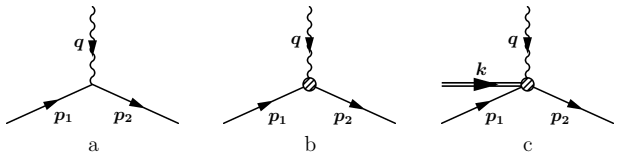

Fig. 1. Photon vertices: a) the local vertex; b, c) quark-photon and quark-photon-meson nonlocal vertices.

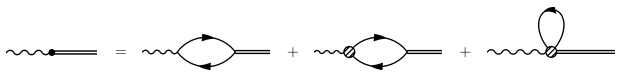

Fig. 2. Diagrams describing vector-meson–photon mixing.

[2] In the description of this section we follow [2].

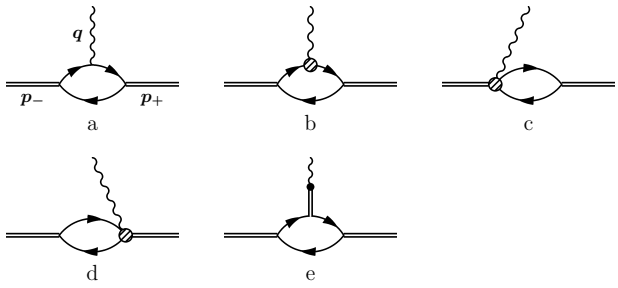

Fig. 3. Diagrams describing the charged-pion radius: a) the local contribution; b-d) nonlocal contributions; e) the diagrams with the ρ-meson.

3 Electromagnetic radius of the charged pion

The diagrams describing the charged-pion radius are presented in fig. 3. The quark loop diagrams with local and nonlocal photon vertices (contact diagrams) are given in the figs. 3a-d and the diagram with the intermediate ρ-meson is drawn in fig. 3e. The amplitude for the process has the form

$$T_{\gamma^*\pi^+\pi^-} = e(p_+ + p_-)^\mu A^\mu(q)\pi^+(p_+)\pi^-(p_-)F_{\gamma^*\pi^+\pi^-}(q^2), \tag{8}$$

where $F_{\gamma^*\pi^+\pi^-}(q^2)$ is the pion form factor and $q = p_+ - p_-$. The electromagnetic pion radius $\langle r^2\rangle_{\rm e.m.}$ is defined by

$$\langle r^2\rangle_{\rm e.m.} = -6\,\frac{{\rm d}F_{\gamma^*\pi^+\pi^-}(q^2)}{{\rm d}q^2}\bigg|_{q^2=0}.$$

In the local NJL model the contact diagram gives about 80% of the correct value for the pion radius [13,15]. Therefore, taking into account the diagram with intermediate ρ-meson [15] leads to a too large value for the pion radius in comparison with the experimental value [22]. Indeed, in the local NJL model one has

$$\begin{aligned}
\langle r^2\rangle^{\rm NJL}_{\rm cont} &= \frac{N_c}{4\pi^2 f_\pi^2} = 0.342\,{\rm fm}^2,\\
\langle r^2\rangle^{\rm NJL}_{\rho} &= 6/M_\rho^2 = 0.394\,{\rm fm}^2,\\
\langle r^2\rangle^{\rm NJL}_{\rm e.m.} &= 0.736\,{\rm fm}^2, \qquad (9)\\
\langle r^2\rangle_{\rm exp} &= 0.451 \pm 0.011\,{\rm fm}^2. \qquad (10)
\end{aligned}$$

Now we show that in contrast, in the nonlocal models the diagram with the intermediate vector meson is noticeably suppressed. In the model considered the contributions to the e.m. pion radius from diagrams in figs. 3a-d and from diagram in fig. 3e equal $\langle r^2\rangle_{\rm cont} = 0.340$ fm^2 and $\langle r^2\rangle_\rho = 0.047$ fm^2, respectively. Then the e.m. pion radius becomes $\langle r^2\rangle_{\rm e.m.} = 0.387$ fm^2, that is in much better agreement with the experimental value than the result of the local model.

Let us consider in more detail the contribution of the ρ-meson diagrams in both the local NJL model and the nonlocal model. These diagrams consist of three parts: the photon–ρ-meson transition, the ρ-meson propagator, and the part describing the $\rho \to \pi\pi$ vertex. Our calculations

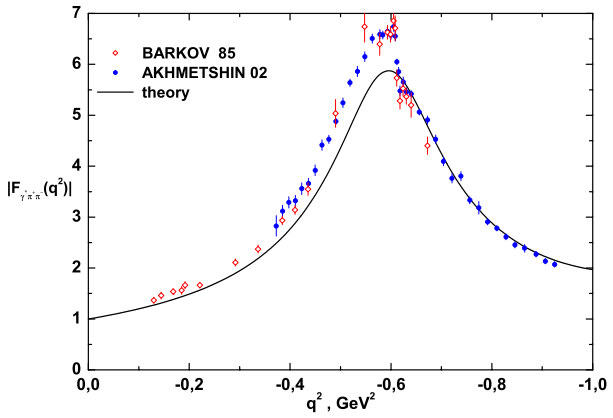

Fig. 4. The absolute value of the charged-pion form factor in the time-like region. The finite width of the ρ-meson is $\Gamma_\rho = 135$ MeV [2]. Experimental data are taken from [23,24].

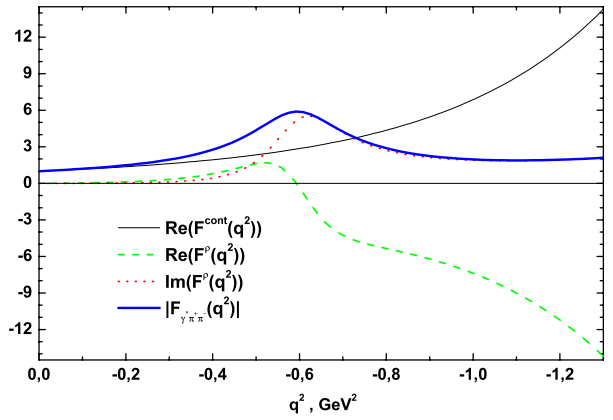

Fig. 5. Partial contributions to the charged-pion form factor in the time-like region from the contact and ρ-meson diagrams and the absolute value of the charged-pion form factor ($\mathrm{Im}(F^{\rm cont}(q^2)) = 0$).

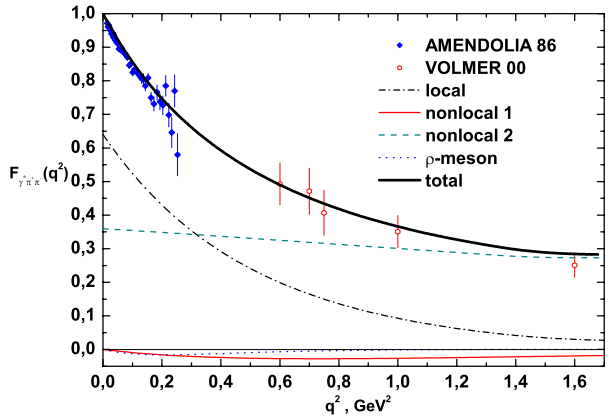

Fig. 6. The charged-pion form factor in the space-like region. Partial contributions from diagrams fig. 3a (local), fig. 3b (nonlocal 1), fig. 3c, d (nonlocal 2), and fig. 3e (ρ-meson) are shown. Experimental data are taken from [25,26].

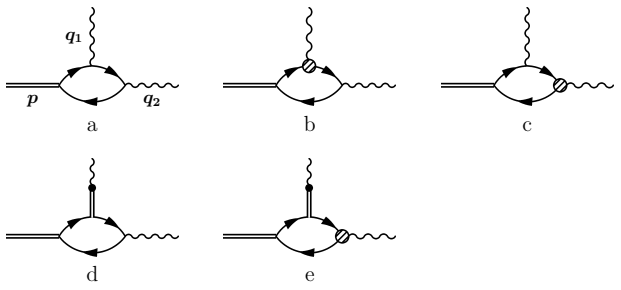

Fig. 7. Diagrams describing the transition neutral pion radius: a) the local contribution; b-c) nonlocal contributions; d, e) the diagrams with vector mesons.

show that in the nonlocal quark models the first part is more than twice smaller than in NJL, the second part does not change, and the third part is four times smaller than in the NJL model. The latter suppression is due to strong q^2-dependence of the amplitude occurring in the nonlocal models. As a result, we obtain almost one-order decrease of the ρ-meson diagram contribution in the nonlocal models with respect to the prediction of the local NJL model.

The charged-pion form factors $F_{\gamma^*\pi^+\pi^-}(q^2)$ in time-like and space-like regions are shown in figs. 4-6. The ρ-meson resonance is displayed in the time-like domain near $-q^2 \approx M_\rho^2$ and we take into account the ρ-meson decay width.

4 Transition radius of the neutral pion

The process $\pi^0 \to \gamma^*\gamma$ is described by the diagrams in fig. 7. Figures 7a-c correspond to the quark loop diagrams with the local and nonlocal photon vertices (contact diagrams), whereas figs. 7d, e correspond to the diagrams with intermediate vector meson. The amplitude of the process has the form

$$T_{\pi_0\gamma\gamma^*} = \frac{e^2}{4\pi^2 f_\pi}\epsilon^{\mu\nu\alpha\beta} q_1^\nu q_2^\mu A^\alpha(q_1) A^\beta(q_2)\pi^0(p) F_{\pi_0\gamma\gamma^*}(q_1^2), \tag{11}$$

where q, q_2, p are the two photon and the pion momentum, respectively. The transition pion radius is defined as[3]

$$\langle r^2\rangle_{\pi_0\gamma\gamma^*} = -6\,\frac{\mathrm{d}F_{\pi_0\gamma\gamma^*}(q_1^2)}{\mathrm{d}q_1^2}\bigg|_{q_1^2=0}. \tag{12}$$

In the local NJL model the contact diagrams give $\langle r^2\rangle^{\rm NJL}_{\rm cont} = 1/2m^2$ [13], where m is the constituent-quark mass. Then in the NJL model without and with the π-a_1 transition one gets $\langle r^2\rangle^{\rm NJL}_{\rm cont} = 0.342$ fm^2 for $m = 240$ MeV and $\langle r^2\rangle^{\rm NJL}_{\rm cont} = 0.248$ fm^2 for $m = 280$ MeV [6], respectively. The experimental value of the transition pion radius is [22]

$$\langle r^2\rangle^{\rm exp}_{\pi_0\gamma\gamma^*} = 0.407 \pm 0.051 \quad \text{fm}^2. \tag{13}$$

[3] The value of the transition pion radius $\langle r^2\rangle_{\pi_0\gamma^*\gamma^*}$ does not depend on the asymmetry $\omega = 2(q_1^2 - q_2^2)/(q_1^2 + q_2^2)$ of photon virtualities q_1^2 and q_2^2. In the case of both off-shell photons the derivative in the definition of radius is taken with respect to the total virtuality of photons.

However, in the local model, the diagrams with vector mesons, figs. 7d, e, again additionally contribute as $\langle r^2\rangle^{\rm NJL}_{\rho+\omega} = 6/M_\rho^2 = 0.394$ fm^2 that noticeably enlarges the value of the transition radius in comparison with experiment.

In contrast, in the nonlocal models the vector meson diagrams are strongly suppressed. Indeed, in the model considered one has $\langle r^2\rangle_{\rm cont} = 0.308$ fm^2 and $\langle r^2\rangle_{\rho+\omega} = 0.07$ fm^2, respectively. Then, we obtain $\langle r^2\rangle_{\pi_0\gamma\gamma^*} = 0.378$ fm^2 that is in satisfactory agreement with experimental data.

We have to note that in the local NJL model the diagram $\rho \to \pi\gamma$ provides $g_\rho/2 \approx 3$ (in the normalization of eq. (11)) and in the nonlocal model it gives ≈ 1.2. Taking into account the value of photon–vector-meson couplings, which are the same as in the case of the charged pion, we see that in the nonlocal models the contribution of vector mesons is more than four times smaller than in the local model.

5 Conclusion

We would like to emphasize that nonlocal models allow us to solve a set of problems that cannot be solved in the local NJL models. First of all it concerns the correct description of momentum dependence of meson amplitudes in the low-energy domain. One of the examples of that is the calculation of electromagnetic meson radii. This problem is considered in present work.

Our calculation is devoted to the investigation of two subjects. First, the region of the effective quark interaction inside the pion is determined. The size of this region corresponds to the electromagnetic and transition radii of the pion. Here, we have shown that in the model considered this region is in agreement with experimental data.

Next, we study relative contributions to the pion form factor $F_{\gamma^*\pi^+\pi^-}$ and pion radii from the contact diagrams and diagrams with vector mesons as intermediate states. We compare these contributions to the pion radii with the results obtained in the framework of the local NJL model. We show that in the nonlocal models the contribution of vector mesons is noticeably smaller than that of the contact diagrams in contrast with the local NJL model where these contributions are comparable. It is worth noting that in the nonlocal models the additional diagrams with photon interacting nonlocally with quark appear. These diagrams are important for gauge invariance. The contributions of the nonlocal contact diagrams to the pion radii have the same order of magnitude as the contributions of the diagrams with vector mesons[4]. Our calculations show that the diagram with local quark-photon vertex gives the dominant part of the pion radii (see table 1).

We have to note finally that one expects further corrections to the pion radii resulted from the so-called $1/N_c$ corrections that are presumably of the same order as the vector meson corrections considered in the present work (see also [14]).

[4] The contribution of the contact diagrams in nonlocal models is comparable with that of local models.

Table 1. The comparison of the pion radii obtained in the nonlocal and local quark models. The local contribution is that from diagrams with local photon vertex (fig. 3a and fig. 7a). The nonlocal contribution is that from diagrams with additional nonlocal photon vertex (figs. 3b-d and figs. 7b, c). The vector meson contributions are those from diagrams with intermediate vector mesons (fig. 3e and figs. 7d, e).

Contribution (fm^2)	$\langle r^2\rangle_{\mathrm{e.m.}}$	$\langle r^2\rangle_{\pi_0\gamma\gamma^*}$	$\langle r^2\rangle^{\mathrm{NJL}}_{\mathrm{e.m.}}$	$\langle r^2\rangle^{\mathrm{NJL}}_{\pi_0\gamma\gamma^*}$
Local	0.302	0.243	0.342	0.342(0.248)
Nonlocal	0.038	0.065		
Vector	0.047	0.07	0.394	0.394
Total	0.387	0.378	0.736	0.736(0.642)

The vector meson diagrams play a very important role in the description of the pion form factor $F_{\gamma^*\pi^+\pi^-}$ in the time-like region. These diagrams allow us not only to describe the ρ-meson resonance but also to obtain a correct behavior of the form factor in the region $-q^2 > M_\rho^2$. It should be noted that the contact and vector meson diagrams increase in absolute values in the region $-q^2 > M_\rho^2$, but they have opposite signs. As a result, the total contribution decreases (see fig. 5) in agreement with the experimental tendency [24].

A similar situation is observed in the nonlocal model considered in [3]. However, in the present model there is an additional relation between model parameters $m(0)$ and Λ, $m(0) = \Lambda$, governed by eq. (3). As a result, arbitrary parameters are absent in contrast to [3]. Nevertheless, in our model the fine-tuning that leads to cancellation of different contributions occurs automatically in accordance with experimental data.

In future, we plan to calculate pion electric and magnetic polarizabilities and π-π scattering lengths.

We are grateful to V.V. Anisovich for drawing our attention to the subject of this work and S.B. Gerasimov for useful discussions. The work is supported by RFBR Grant No. 02-02-16194 and the Heisenberg-Landau program. A.E.D. acknowledges partial support from RFBR (Grants Nos. 01-02-16431, 03-02-17291) and INTAS (Grant No. 00-00-366).

Appendix A.

Here we present the vertices used in the above calculations. The nonlocal quark-photon vertex is

$$-eQ(p_1+p_2)^\mu \frac{m(p_1)-m(p_2)}{p_1^2-p_2^2}\bar q(p_1)q(p_2)A_\mu(p_1-p_2), \tag{A.1}$$

while the nonlocal quark-photon-meson vertex takes the form

$$\begin{aligned} &e\bar q(p_1)q(p_2)A_\mu(q)g_M(k)M(k)\\ &\quad\times\left(\frac{f(p_1)-f(p_1+q)}{p_1^2-(p_1+q)^2}f(p_2)(2p_1+q)^\mu Q\Gamma_M\right.\\ &\quad\left.+\frac{f(p_2)-f(p_2-q)}{p_2^2-(p_2-q)^2}f(p_1)(2p_2-q)^\mu\Gamma_M Q\right), \end{aligned} \tag{A.2}$$

where q, k, p_1, $p_2 = p_1+q+k$ are the momenta of the photon, meson, antiquark and quark, respectively; M is the meson field; g_M is the function describing the renormalization of the meson field; the matrices Γ_M are defined by

$$\Gamma_\pi^a = i\gamma^5\tau^a, \quad \Gamma_\rho^{\mu\,a} = \gamma^\mu\tau^a, \quad \Gamma_\omega^\mu = \gamma^\mu.$$

References

1. A.E. Dorokhov, A.E. Radzhabov, M.K. Volkov, Phys. At. Nucl. **67**, (2004).
2. A.E. Radzhabov, M.K. Volkov, Part. and Nucl., Lett. **1[118]**, 5 (2004); Eur. Phys. J. A **19**, 341 (2004).
3. R.D. Bowler, M.C. Birse, Nucl. Phys. A **582**, 655 (1995); R.S. Plant, M.C. Birse, Nucl. Phys. A **628**, 607 (1998).
4. A.E. Dorokhov, L. Tomio, Phys. Rev. D **62**, 014016 (2000), arXiv:hep-ph/9803329; I.V. Anikin, A.E. Dorokhov, L. Tomio, Phys. Part. Nucl. **31**, 509 (2000).
5. A.E. Dorokhov, W. Broniowski, Phys. Rev. D **65**, 094007 (2002).
6. M.K. Volkov, Sov. J. Part. Nuclei **17**, 186 (1986).
7. M.K. Volkov, D. Ebert, Yad. Fiz. **36**, 1265 (1982); M.K. Volkov, Ann. Phys. (N.Y.) **157**, 282 (1984); D. Ebert, H. Reinhardt, Nucl. Phys. B **271**, 188 (1986); U. Vogl, W. Weise, Prog. Part. Nucl. Phys. **27**, 195 (1991); S.P. Klevansky, Rev. Mod. Phys. **64**, 649 (1992).
8. E.V. Shuryak, Nucl. Phys. B **203**, 93 (1982).
9. D. Diakonov, V.Y. Petrov, Nucl. Phys. B **245**, 259 (1984); **272**, 457 (1986).
10. A.E. Dorokhov, N.I. Kochelev, JINR-E2-86-224; A.E. Dorokhov, Y.A. Zubov, N.I. Kochelev, Sov. J. Part. Nucl. **23** , 522 (1992).
11. A.E. Dorokhov, W. Broniowski, Eur. Phys. J. C **32**, 79 (2003), arXiv:hep-ph/0305037.
12. I.V. Anikin, A.E. Dorokhov, L. Tomio, Phys. Lett. B **475**, 361 (2000); A.E. Dorokhov, JETP Lett. **77**, 63 (2003) (Pis'ma Zh. Eksp. Teor. Fiz. **77**, 68 (2003)).
13. S.B. Gerasimov, Yad. Fiz. **29**, 513 (1979).
14. H.J. Hippe, S.P. Klevansky, Phys. Rev. C **52**, 2172 (1995).
15. M.K. Volkov, Phys. At. Nucl. **60**, 997 (1997).
16. R. Tarrach, Z. Phys. C **2**, 221 (1979).
17. V. Bernard, U.G. Meissner, Phys. Rev. Lett. **61**, 2296 (1988); **61**, 2973 (1988)(E).
18. M. Lutz, W. Weise, Nucl. Phys. A **518**, 156 (1990).
19. J. Terning, Phys. Rev. D **44**, 887 (1991).
20. G.V. Efimov, M.A. Ivanov, *The Quark Confinement Model of Hadrons* (IOP, Bristol, 1993).
21. A.E. Dorokhov, arXiv:hep-ph/0212252.
22. Particle Data Group Collaboration (K. Hagiwara *et al.*), Phys. Rev. D **66**, 010001 (2002).
23. L.M. Barkov *et al.*, Nucl. Phys. B **256**, 365 (1985).
24. CMD-2 Collaboration (R.R. Akhmetshin *et al.*), Phys. Lett. B **527**, 161 (2002); *Reanalysis of hadronic cross-section measurements at CMD-2*, Phys. Lett. B **578**, 285 (2004), arXiv:hep-ex/0308008.
25. NA7 Collaboration (S.R. Amendolia *et al.*), Nucl. Phys. B **277**, 168 (1986).
26. The Jefferson Lab F(pi) Collaboration (J. Volmer *et al.*), Phys. Rev. Lett. **86**, 1713 (2001).